

Influence of structural modifications on the alkali ion storage properties of carbon black in hybrid ion capacitor negative electrodes

Supporting Information

J. Schenk,¹ D. Leistenschneider,^{1,2} S. Hoeppener,^{2,3} U. S. Schubert,^{2,3} K. Schutjajew,¹ M. Oschatz^{1,2}

¹ Institute for Technical Chemistry and Environmental Chemistry, Friedrich Schiller University Jena, Philosophenweg 7a, 07743 Jena, Germany.

² Center for Energy and Environmental Chemistry Jena (CEEC Jena), Philosophenweg 7a, 07743 Jena, Germany.

³ Laboratory of Organic and Macromolecular Chemistry (IOMC), Friedrich Schiller University Jena, Humboldtstrasse 10, 07743 Jena, Germany.

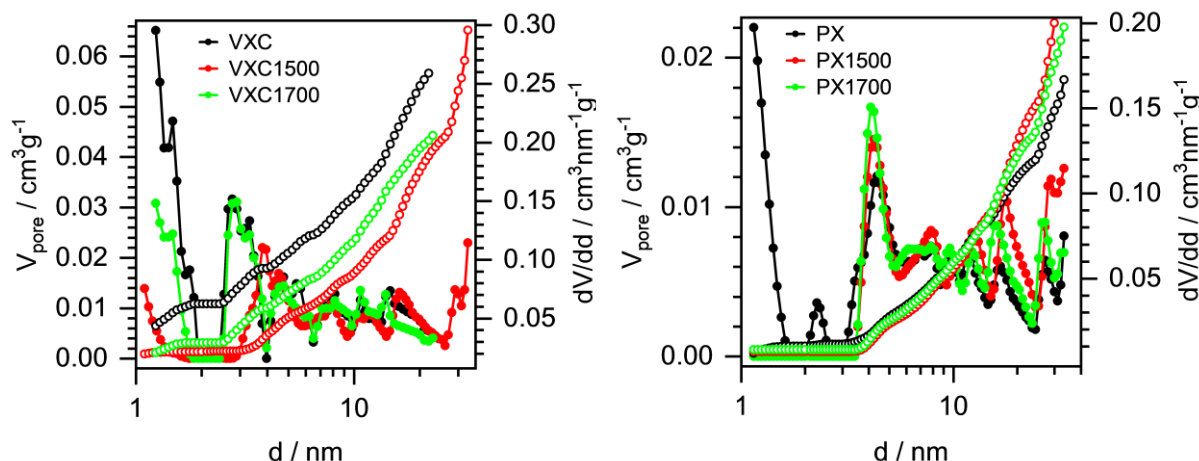


Fig. S1: Pore size distributions derived from QSDFT for slit/cylindrical pores in N_2 physisorption (adsorption branch) at 77 K.

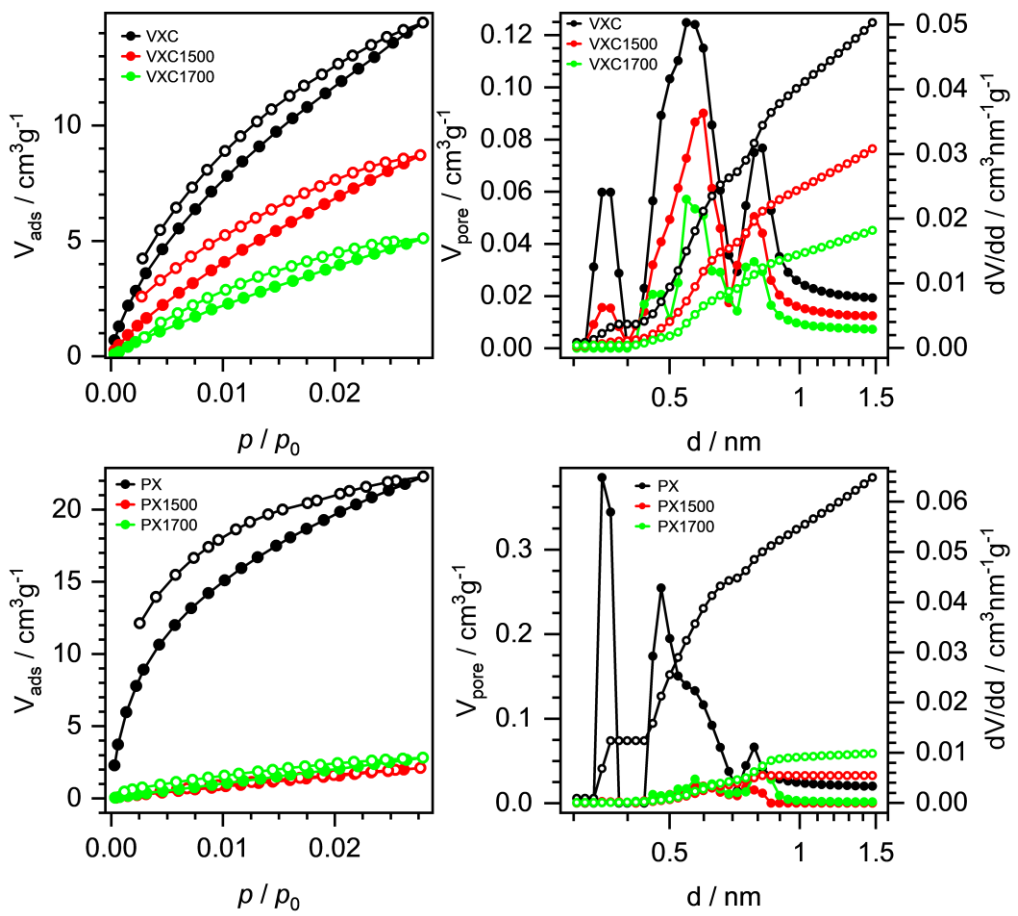


Fig. S2: CO_2 isotherms at 273 K and the corresponding NLDFT calculated pore size distributions.

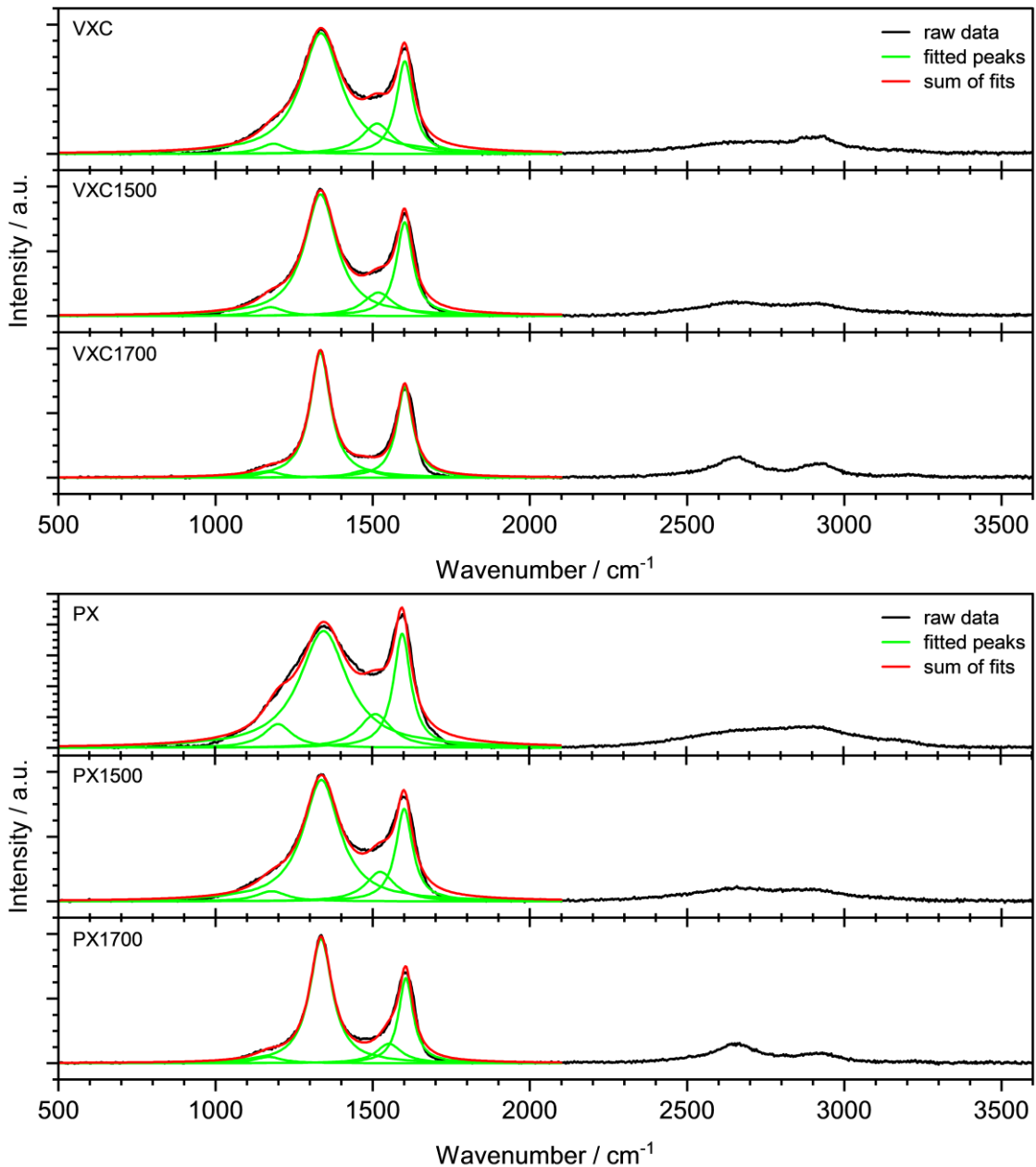


Fig. S3: Raman spectra with the corresponding fitted peaks and sum of fits for VXC, PX and HTT CBs.

Table S1: Intensity ratios of D- and G-band from Raman spectroscopy.

	VXC	VXC1500	VXC1700	PX	PX1500	PX1700
I_D / I_G	1.30	1.30	1.38	1.02	1.31	1.46

Table S2: Full width at half maximum (FWHM) and peak position of the (002) reflection derived from XRD.

	VXC	VXC1500	VXC1700	PX	PX1500	PX1700
FWHM (002)	5.0	3.9	2.8	6.5	4.9	3.7
2θ (002)	24.4	24.8	25.2	24.0	24.5	25.0

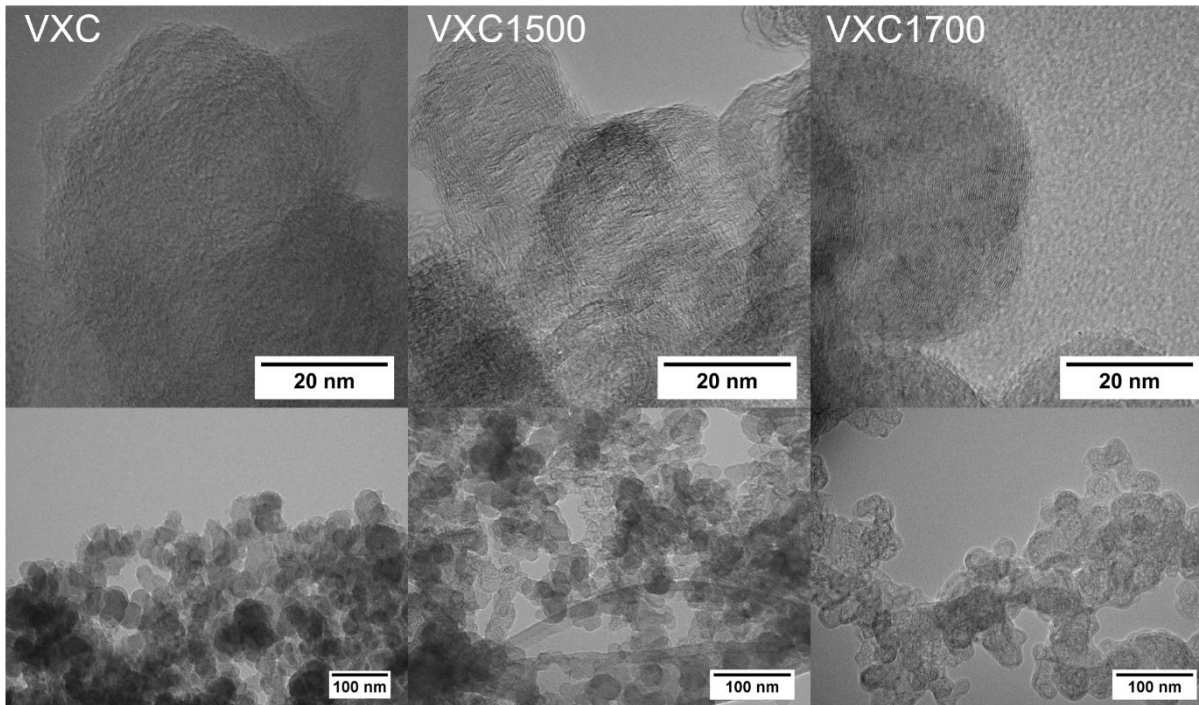


Fig. S4: TEM images of VXC, VXC1500 and VXC1700 with different magnifications.

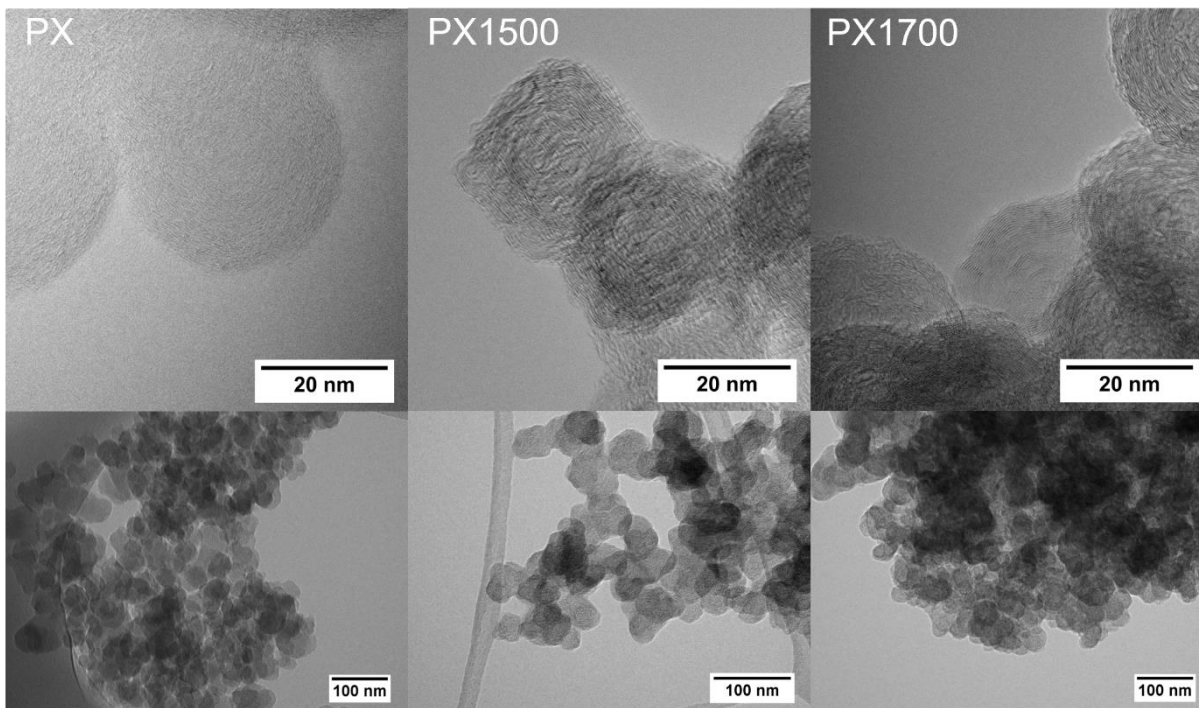


Fig. S5: TEM images of PX, PX1500 and PX1700 with different magnifications.

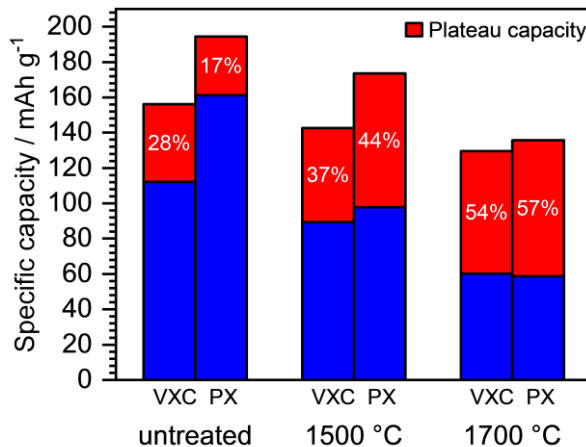


Fig. S6: Overall specific capacity and contribution of plateau capacity in relation to the treatment temperature of the two carbon black materials for sodium ion half-cells.

Table S3: Atomic contents of different binding energy signals of C1s, Na1s and F1s spectra of the cycled electrodes of a) VXC and b) VXC1700.

a)

C1s			
Binding energy / eV	FWHM / eV	Area / cps	Atomic %
284.68	1.54	26989.2	52.3
283.43	0.76	8017.12	15.52
289.83	1.38	6683.24	12.99
286.64	1.46	7243.32	14.05
288.57	1.3	2636.96	5.12
Na1s			
Binding energy / eV	FWHM / eV	Area / cps	Atomic %
1071.45	1.3	28534.51	53.36
1072.08	1.5	24918.12	46.64
F1s			
Binding energy / eV	FWHM / eV	Area / cps	Atomic %
687.33	1.74	25259.65	88.86
684.37	1.4	3176.47	11.14

b)

C1s			
Binding energy / eV	FWHM / eV	Area / cps	Atomic %
284.6	1.56	61469.8	69.2
283.6	0.65	9038.1	10.2
286.7	1.72	10113.9	11.4
289.7	1.78	6392.6	7.2
288.5	0.98	1851.0	2.1
Na1s			
Binding energy / eV	FWHM / eV	Area / cps	Atomic %
1071.4	1.24	17154.2	37.6
1071.9	1.52	28492.6	62.4
F1s			
Binding energy / eV	FWHM / eV	Area / cps	Atomic %
684.2	1.52	2477.1	16.8
687.5	1.75	12241.1	83.2

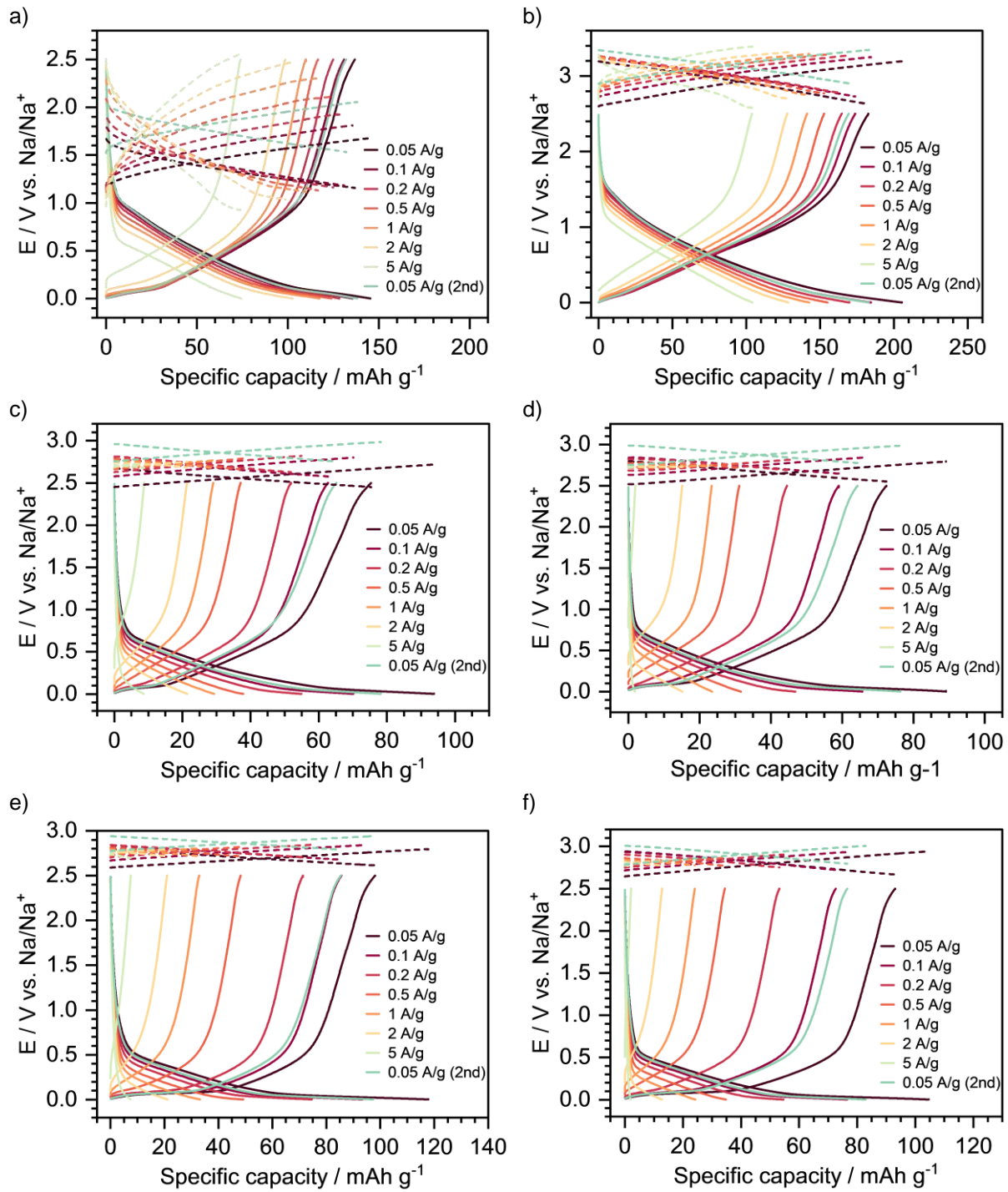


Fig. S7: Galvanostatic charge-discharge curves of the fifth cycle of each current density measured in SIC setup. The carbon black electrodes a) VXC, b) PX, c) VXC1500, d) PX1500, e) VXC1700 and f) PX1700 are depicted in solid lines. The corresponding activated carbon counter electrodes are shown in dashed lines.

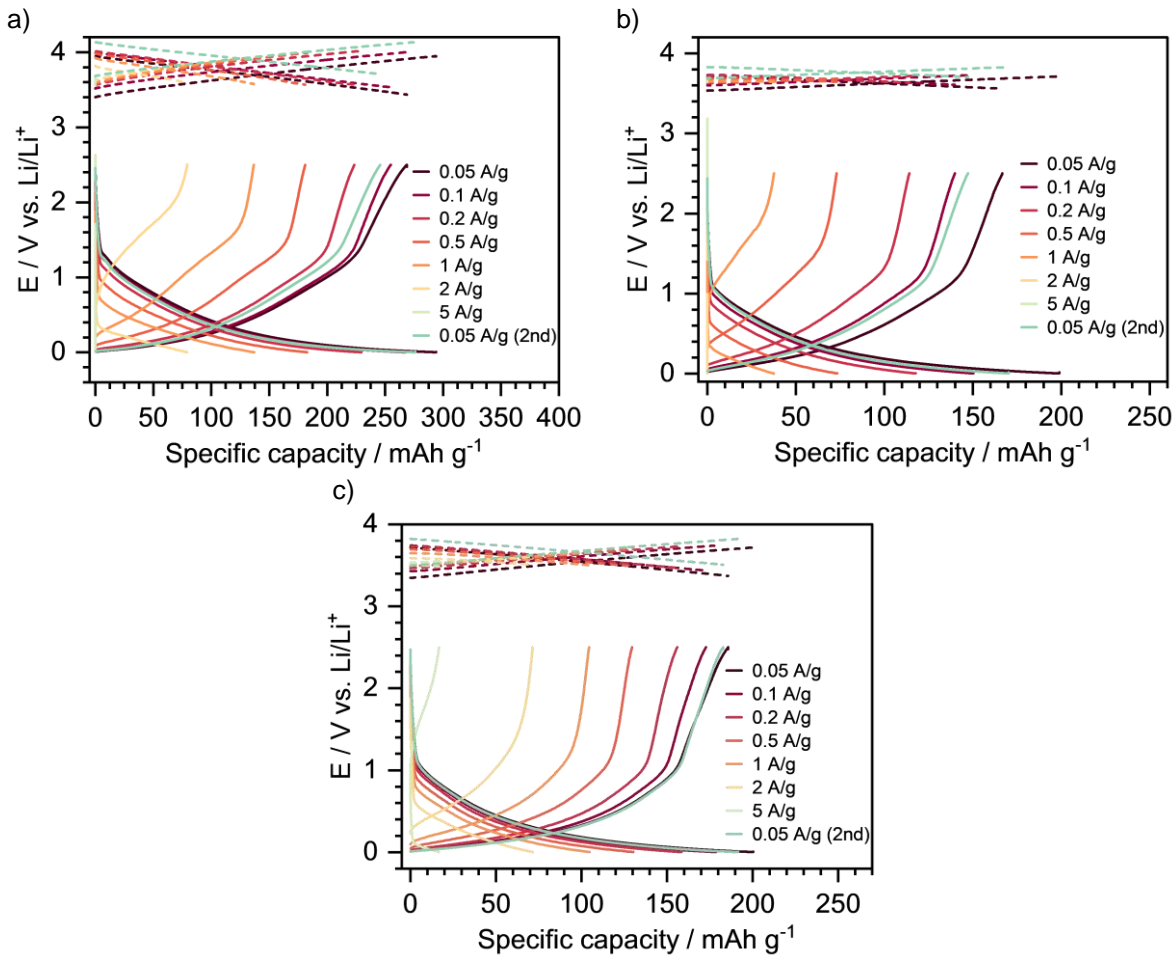


Fig. S8: Galvanostatic charge-discharge curves of the fifth cycle of each current density measured in LIC setup. The carbon black electrodes a) VXC, b) VXC1500 and c) VXC1700 are depicted in solid lines. The corresponding activated carbon counter electrodes are shown in dashed lines.

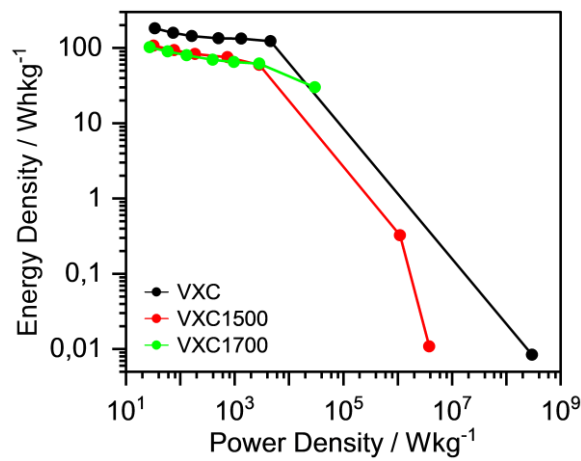


Fig. S9: Ragone plot of VXC samples in LIC.

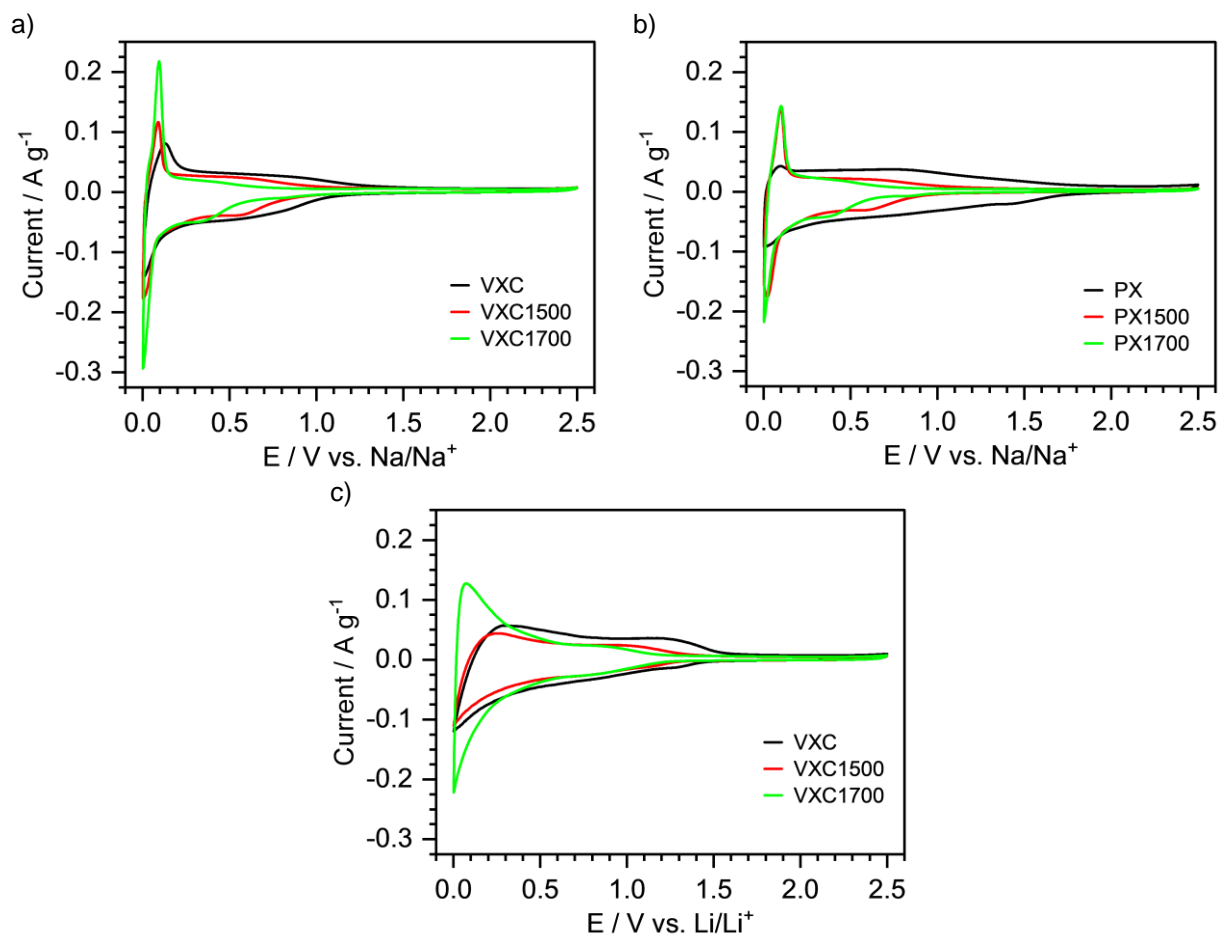


Fig. S10: Cyclic voltammograms at 0.1 mV s⁻¹ for a) VXC, VXC1500 and VXC1700 and b) PX, PX1500 and PX1700 in SIC and c) VXC, VXC1500 and VXC1700 in LIC.

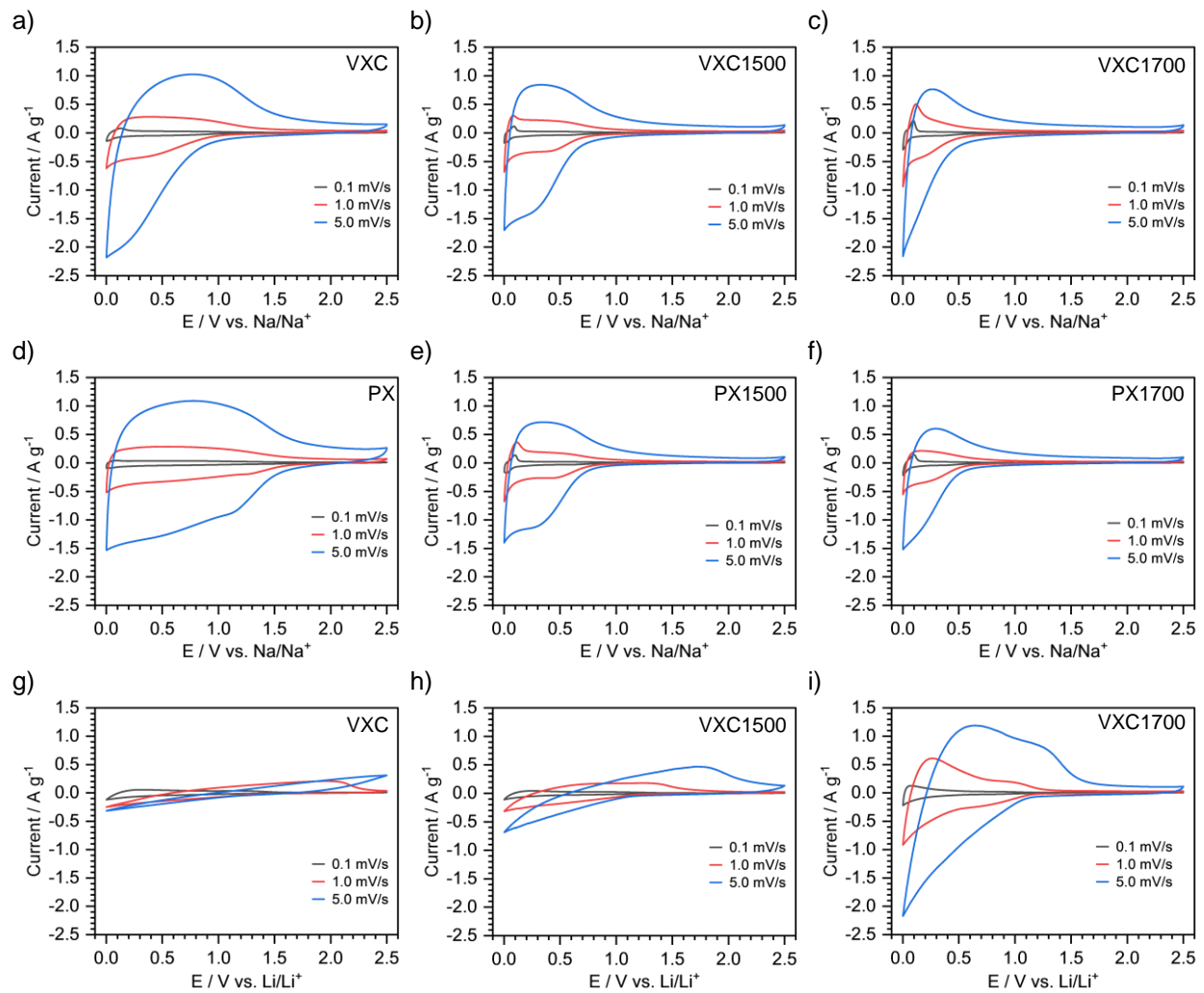


Fig. S11: Cyclic voltammograms at different scan rates a) to f) in SIC and g) to i) in LIC.

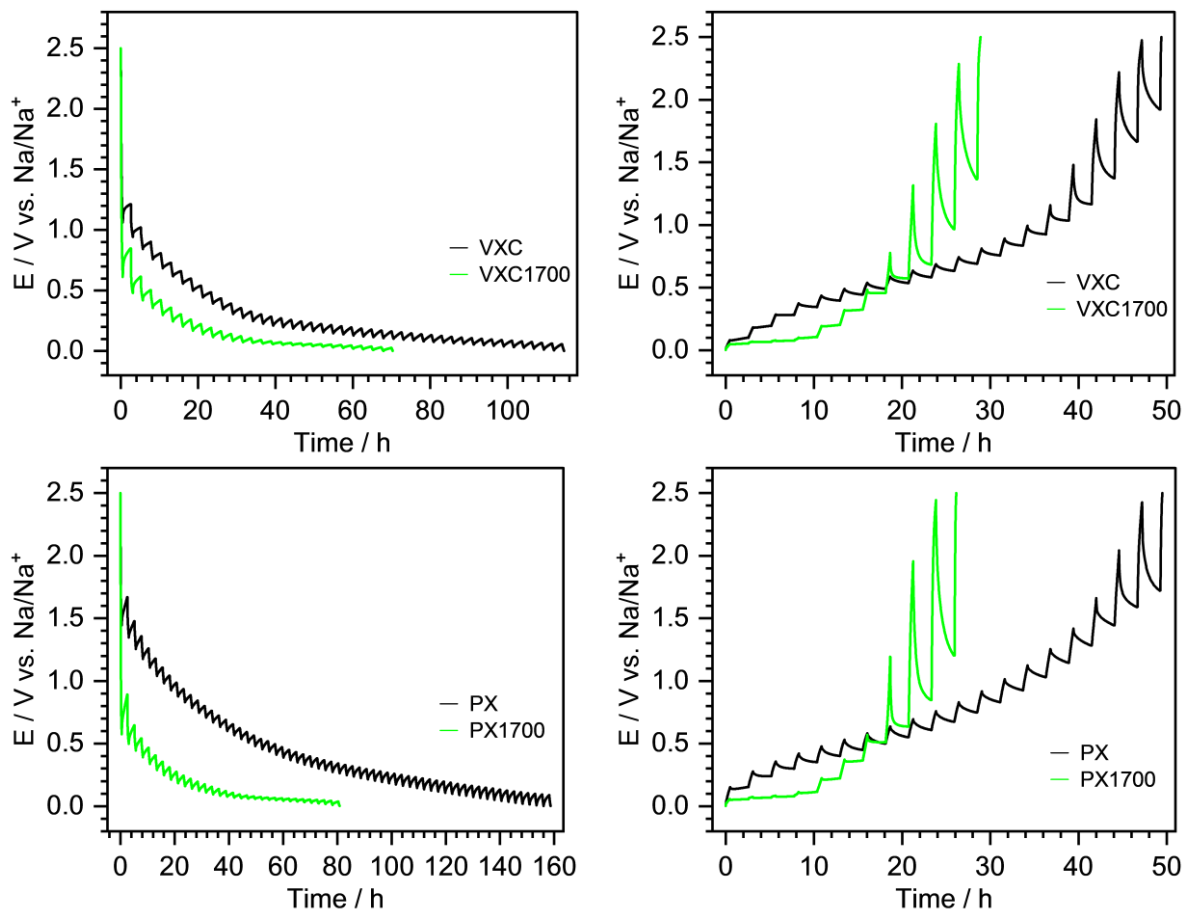


Fig. S12: Potential profile of GITT measurements.

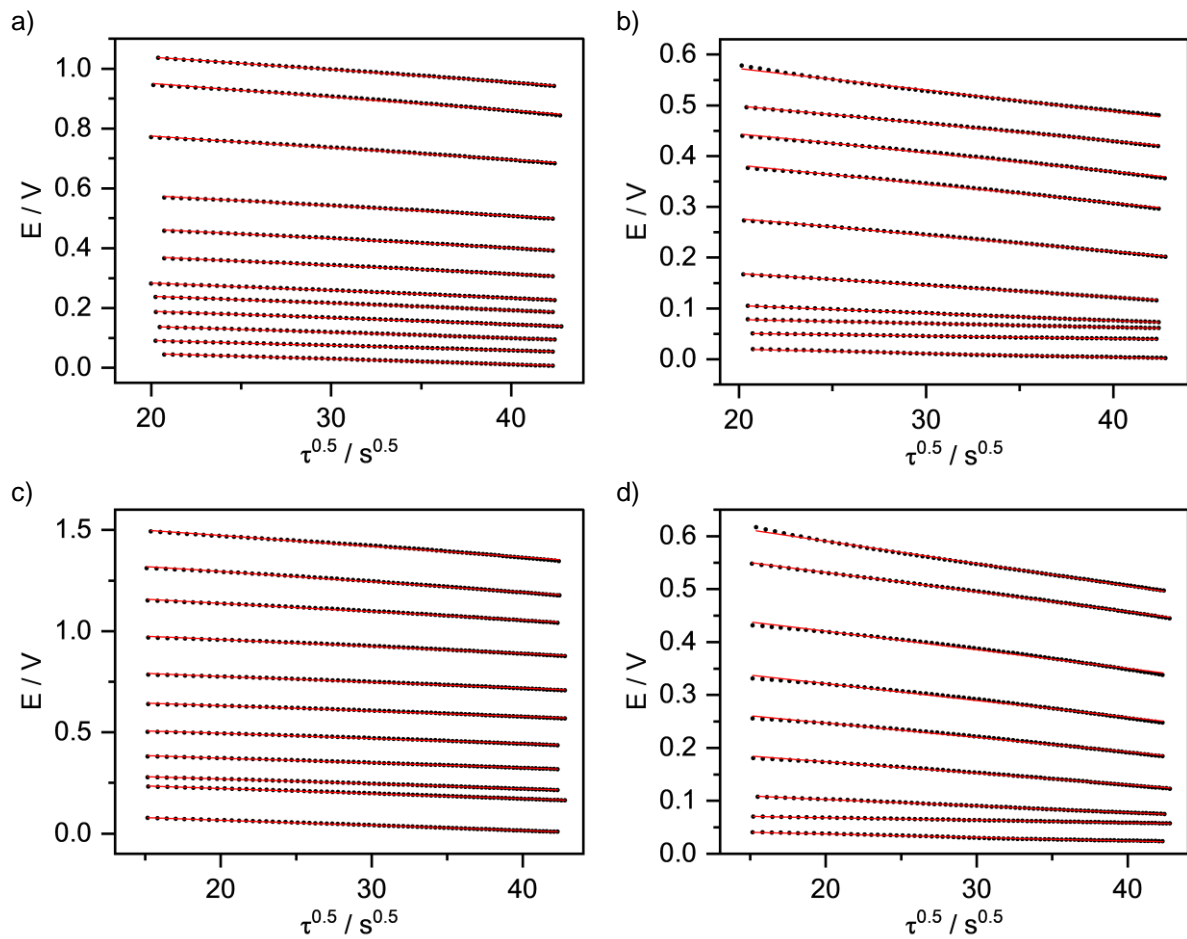


Fig. S13: Potential vs. $\tau^{0.5}$ with linear fitting of a) VXC, b) VXC1700, c) PX and d) PX1700.